Published in final edited form as:
*Exp Cell Res*. 2008 April 15; 314(7): 1540–1552. doi:10.1016/j.yexcr.2008.01.016.

# RhoA/ROCK-mediated switching between Cdc42- and Rac1-dependent protrusion in MTLn3 carcinoma cells

**Mirvat El-Sibai**[1], **Olivier Pertz**[4], **Huan Pang**[1], **Shu-Chin Yip**[1], **Mike Lorenz**[2], **Marc Symons**[2,3], **John S. Condeelis**[2,6], **Klaus M. Hahn**[5], and **Jonathan M. Backer**[1,*]

1 *Molecular Pharmacology, Albert Einstein College of Medicine, 1300 Morris Park Avenue, Bronx, NY 10461, USA*

2 *Anatomy and Structural Biology, Albert Einstein College of Medicine, 1300 Morris Park Avenue, Bronx, NY 10461, USA*

3 *Center for Oncology and Cell Biology, The Feinstein Institute for Medical Research at North Shore-LIJ, North Shore University Hospital, Manhasset, NY 11030, USA*

4 *Immunology, Scripps Research Institute, 10550 North Torrey Pines Road La Jolla, CA 92037, USA*

5 *Pharmacology, University of North Carolina School of Medicine CB7365, Chapel Hill, NC27599, USA*

6 *Analytical Imaging Facility, Albert Einstein College of Medicine, Bronx, NY10461*

## Abstract

Rho GTPases are versatile regulators of cell shape that act on the actin cytoskeleton. Studies using Rho GTPase mutants have shown that, in some cells, Rac1 and Cdc42 regulate the formation of lamellipodia and filopodia, respectively at the leading edge, whereas RhoA mediates contraction at the rear of moving cells. However, recent reports have described a zone of RhoA/ROCK activation at the front of cells undergoing motility. In this study, we use a FRET-based RhoA biosensor to show that RhoA activation localizes to the leading edge of EGF-stimulated cells. Inhibition of Rho or ROCK enhanced protrusion, yet markedly inhibited cell motility; these changes correlated with a marked activation of Rac-1 at the cell edge. Surprisingly, whereas EGF-stimulated protrusion in control MTLn3 cells is Rac-independent and Cdc42-dependent, the opposite pattern is observed in MTLn3 cells after inhibition of ROCK. Thus, Rho and ROCK suppress Rac-1 activation at the leading edge, and inhibition of ROCK causes a switch between Cdc42 and Rac-1 as the dominant Rho GTPase driving protrusion in carcinoma cells. These data describe a novel role for Rho in coordinating signaling by Rac and Cdc42.

### Keywords

RhoA; ROCK; Rac; EGF; metastasis

* Corresponding Author: Jonathan M. Backer, M.D. Department of Molecular Pharmacology, Albert Einstein College of medicine, 1300 Morris Park Avenue, Bronx, NY 10461, Tel: (718) 430 - 2124, Fax: (718) 430 - 3749, E-mail: backer@aecom.yu.edu.

## Introduction

Motility is a fundamental property of cells and is essential for physiological and pathological events, including embryonic development, immune responses, wound healing, and tumor metastasis. Motility towards a chemoattractant starts with the initial detection of a chemoattractant source, which leads to the reorientation of the intracellular signaling machinery such that the cell is committed to a given direction [1]. This is followed by the localized extension of an actin-rich structure, such as a lamellipod, which propels the cell towards the chemoattractant [2]. The steps that follow include adhesion of the lamellae to the extracellular matrix, development of contractile force, de-adhesion of focal adhesions at the tail of the cell, and contraction causing tail retraction toward the leading lamellae [3].

Rho family GTPases are molecular switches that couple the detection of chemoattractants to actin polymerization [4]. Studies using constitutively active and dominant negative forms of Rho GTPases have shown that, in some cells, Rac1, Cdc42 and Rho regulate the formation of lamellipodia, filopodia and stress fibers, respectively [5]. Rac1 and Cdc42 regulate actin polymerization through the indirect or direct activation of Scar/WAVE and WASP/N-WASP nucleation promoting factors that activate the Arp2/3 complex [6,7]. Rho also plays a positive role in the regulation of cell motility. Indeed, the inhibition of Rho, through the microinjection of the Rho inhibitor, *Clostridium botulinum* ADP-ribosyltransferase C3 (C3T), inhibits cell motility in many cell systems [8,9]. Initially, the role of RhoA during cell motility was thought to be restricted to the generation of contractile force and focal adhesion turnover needed for tail retraction [10,11]. This is achieved through its downstream effector, the serine/threonine kinase p160ROCK, which leads to myosin phosphorylation and actin-myosin contractility [12]. Based on the antagonism between Rho/ROCK and Rac, it was originally postulated that RhoA activity at the front of a migrating cell was incompatible with membrane protrusion [10,13].

This model has been challenged by recent studies using fluorescence-based biosensors and other methods to visualize the subcellular distribution of Rho GTPase activity [14–16]. Recent reports have described a zone of RhoA/ROCK activation at the leading edge of cells [14,17–19]. Although the precise role of RhoA at the leading edge of cells is still elusive, many downstream effectors from RhoA could be directly involved in cell protrusion. Through ROCK, RhoA leads to focal adhesion formation, which stabilizes the leading lamellae during cell protrusion [20]. ROCK is required for myosin-based contractility at the front of invading carcinoma cells [21]. RhoA/ROCK also phosphorylates and activates LIMK and could lead to cofilin inhibition and actin filament stabilization [22]. Finally, RhoA signals to mDia, a potent actin nucleator that could play a role in lamellipod formation [23].

In this report we examine the role of the Rho/p160ROCK pathway during actin-based protrusion in EGF-stimulated carcinoma cells. We show that RhoA activation is kinetically correlated with actin nucleation, and occurs in a broad band that extends throughout the protruding lamellipod and into the lamellar region. Inhibition of Rho or p160ROCK leads to increased protrusion but decreased motility. Moreover, inhibition of ROCK leads to a switch in the Rho GTPase that regulates protrusion: protrusion in control MTLn3 requires Cdc42 but not Rac, whereas protrusion in cells treated with ROCK inhibitor requires Rac-1 but not Cdc42. Thus, activation of Rho/ROCK at the cell edge coordinates the coupling of Cdc42 and Rac-1 to the actin cytoskeleton.

## Materials and Methods

### Cell Culture

Rat mammary adenocarcinoma cells, MTLn3 cells, were cultured in α-MEM media supplemented with 5% FBS as previously described [24]. MTC cells expressing the human EGF receptor have been previously described [25]. For microscopy experiments, cells were plated on coverslips coated with rat tail type 1 collagen (BD Biosciences, Bedford MA) or on collagen-coated dishes (MatTek Corporation) 24 hours prior to the experiment. The cells were then starved in L15 media (GIBCO BRL) with 0.35% BSA for 3 hours, and stimulated with a final concentration of 5nM murine epidermal growth factor for various times (EGF; Upstate biotechnology, Lake Placid, NY).

### Antibodies and reagents

Mouse monoclonal anti-Rho antibody (clone 55), rabbit monoclonal anti-Rho antibody (clone 3L74), mouse monoclonal anti-Rac antibody (clone 23A8), and the mouse monoclonal anti-Paxillin (clone 5H11) were purchased from Upstate Biotechnology. The rabbit polyclonal anti-Cdc42 antibody (sc-87) was obtained from Santa Cruz Biotechnology (Santa Cruz, CA). The Cy5-conjugated anti-biotin was obtained from Jackson ImmunoResearch Laboratories (West Grove, PA). Rhodamine Phalloidin, Alexa fluor 488-conjugated Dextran and fluorescent secondary antibodies were obtained from Molecular Probes (Eugene, OR). The ROCK inhibitor, Y27632, was obtained from Calbiochem-Novabiochem Co (San Diego, CA). The selective myosin II inhibitor, blebbistatin, was purchased from Sigma (St Louis, MO). Wild type Rac and RacQ61L were in eGFP-pcDNA3 vectors. The GFP-Vinculin was a generous gift from Dr. Stefan Huettelmaier.

### Cell Transfection with small interfering RNA

Rac1 siRNA [26] and Cdc42 siRNA[27] were previously described. The Rac1 siRNA oligo was: 5′-AAAGAGAUCGGUGCUGUCAAA-3′. Alternatively, a collection of four siRNA (Dharmicon Smartpools) was used. The Cdc42 siRNA oligo was: 5′-AAAGACTCCTTTCTTGCTTGT-3′. MTLn3 cells were transfected with 100nM Rac or Cdc42 siRNA or with control siRNA sequences targeting GL2 luciferase[28] (Ambion) for 48 hours prior to the day of the experiment using Oligofectamine (Invitrogen) as described by the manufacturer. Rac and Cdc42 suppression of protein levels was analyzed by Western blotting using antibodies against total Rac and Cdc42 respectively.

### Protein purification

pGEX-2T human PAK GTPase-binding domain (hPAK residues 67–150, CRIB domain), pGEX-2T RhoA binding domain of Rhotekin (residues 7–89, RBD), pGEX-full length C3 transferase (Rho inhibitor, C3T a generous gift from Dr. Judy Meinkoth, Univ. Pennsylvania) and the pGEX-full length Rho were expressed in *Escherichia Coli* as GST fusion proteins. The proteins were purified by binding to glutathione-Sepharose (Amersham Biosciences). The purity and concentration of the proteins was determined by SDS-PAGE and Coomassie Blue staining.

### Pull-down assays and Western Blots

MTLn3 cells were starved for 3 hours, stimulated with EGF for various times and stopped by the addition of ice cold PBS containing with 1 mM sodium orthovanadate. The cells were lysed and incubated with GST-CRIB (for Rac) or GST-RBD (for Rho). Rho and Rac were detected by Western Blotting using the anti-Rho (rabbit) and anti-Rac antibodies, and imaged and quantitated using a LICOR Odyssey system.

### C3T inhibition of Rho

Cells were microinjected using an Eppendorf 5171/5242 semi-automatic micromanipulator/microinjector. MTLn3 cells were starved for 2 hours then injected with 150 μg/ml of the C3T protein along with Alexa fluor 488-conjugated Dextran or with 150 μg/ml IgG in PBS. The cells were left to recover for 1 hour then stimulated with EGF.

### Immunofluorescence

After EGF stimulation, cells were permeabilized with saponin and fixed as previously described[29] for 30 min at 37°C. Cells were then rinsed with PBS, and aldehyde autofluorescence was quenched with 1mg/ml $NaBH_4$. For blocking, cells were incubated with 1% BSA/1%FBS in PBS for 30 min. Cells were stained with primary antibodies for 2 hours and with secondary antibodies for 2 hours. For the pre-absorption experiments, cells were stained with anti-Rho (mouse) pre-incubated in solution with GST alone or with GST-RhoA for 1 hr at 4°C prior to staining. All fluorescent images were taken using a 60 X 1.4 NA infinity-corrected optics on a Nikon Eclipse microscope supplemented with a computer-driven Roper cooled CCD camera and operated by IPLab Spectrum software (VayTek). We have previously shown, using atomic force microscopy, that the height of the lamellipod in EGF-stimulated MTLn3 cells is approximately 600–800 nm (Rotsch et al., 2001). Thus, the entire lamellipod is within one optical section and the use of confocal microscopy was not necessary. For image analysis, all digital images were imported in image J software (National Institutes of Health, USA). For fluorescent quantification, images were analyzed using a previously described macro [30].

### Live upshift and motility assay

For live protrusion analysis, starved cells were stimulated with EGF and analyzed by time-lapse microscopy every 20 seconds. For motility analysis, images were collected every 60 seconds for 2 hours using a 20X objective in serum and their rate of movement quantitated using ImageJ and DIAS computational software [31]. Optimal temperature and $CO_2$ control were maintained using an inverted Olympus IX70 microscope mounted in an incubation chamber.

### RhoA FRET biosensor imaging and analysis

MTLn3 cells were transfected with 1μg of the RhoA fluorescence resonance energy transfer (FRET)-based biosensor plasmid [14], which shows an increase in FRET ratio with GTP-loading of RhoA, using Fugene6 (Roche, Switzerland) for 24 hr as described by the manufacturer. The biosensor consists of (from the N-terminus) the Rho binding domain (RBD) of the effector Rhotekin, a cyan fluorescent protein (CFP), a protease resistant 17mer unstructured linker, a yellow florescent protein (YFP) domain, and a full length RhoA [14]. Activation of RhoA can be determined as a ratio of the FRET image over the CFP image [32]. FRET image sequences were obtained with an automated Olympus IX70 microscope equipped with filter wheels in the excitation and emission light path and coupled to a cooled SensiCam QE CCD camera (Cooke Corp., MI). CFP was excited using a S430/25 filter with a Sutter DG4 illuminator (Sutter Instruments, Novato, CA) and the fluorescence detected with a S470/30 (donor image) or S535/30 (FRET image) emission filter. YFP was imaged with exciter S500/20 and emitter S535/30 (YFP image). In all cases a dual-band dichroic mirror 86002v2bs was used (Chroma Technology Corp., VT). Images were background corrected and the YFP images were thresholded to generate a binary mask with values of 1 within the cell and 0 for the background. Similar results were obtained when the mask was generated using the YFP image to define the cell edge. This was used to remove the background from ratio calculations, by multiplying CFP and FRET images by the mask. The increase in FRET signal due to activation of RhoA was detected by dividing the FRET image (CFP excitation- YFP

emission) by the donor image (CFP excitation- CFP emission). Acquisition and FRET analyses were done with IP Lab v3.51 (Scanalytics Inc., VA). Live FRET time-lapse movies were collected using a DualView image splitter (Optical Insights, LLC, Tucson, AZ). The live imaging was done with 4X4 binning to minimize exposure time, photobleaching and registration artifacts. FRET signals were quantified by averaging the mean FRET ratio in regions of interest in cells stimulated for various times. Procedures were based on those previously described [14].

## Results

### Spatial and temporal analysis of Rho activation in EGF-stimulated carcinoma cells

In order to understand the involvement of RhoA in the events leading to cell protrusion, we studied the kinetics and subcellular distribution of RhoA activation in MTLn3 carcinoma cells; expression of RhoC is undetectable by western blot in these cells (data not shown). The activation of total cellular Rho was examined in a pull-down assay using GST fused to the Rho binding domain (RBD) from Rhotekin [33]. In EGF-stimulated MTLn3 cells, Rho followed a biphasic activation profile (Fig 1A), with an initial peak of activation at 60 seconds. Rho activation dropped to near basal levels by 100 seconds, but then increased again after 180 seconds of EGF stimulation. These kinetics coincide with the kinetics of actin polymerization in MTLn3 cells, which also shows transients at 1 and 3 minutes [2]. Interestingly, the localization of Rho at 1 versus 3 min was different. At 1 min, Rho was localized to a narrow band that extended approximately 0.5 μm into the cell (Fig 1B middle panel), which is the zone of f-actin accumulation in EGF-stimulated MTLn3 cells [34]. We presume that this is staining pattern is largely due to RhoA, since RhoB is confined to endosomes [35]. However, by 3 minutes, anti-Rho staining is localized to a broader region that began approximately 0.5 μm behind the leading edge and extended 2 μm into the cell (Fig. 1B right panel). Previous studies have suggested that this zone includes the tropomyosin-rich lamellar region [30,36]. Anti-Rho staining was also observed in numerous punctate structures, which could result from RhoB in endosomal structures. These data are consistent with previous observations of a small fraction of RhoA in the plasma membrane [35]. Anti-Rho staining was specific, as it was abolished by pre-absorption with GST-RhoA (Fig 1C) but not GST (data not shown).

To directly visualize active RhoA in carcinoma cells, we used a single chain CFP/YFP FRET biosensor (Fig. S1A) [14]. Control experiments demonstrated that the probe for RhoA activation is inhibited by microinjection of C3T (Fig S1B and S1C), and that biosensor expression does not perturb EGF-stimulated cytoskeletal responses (S1D). Analysis of the FRET signal at various probe expression levels revealed a slight increase at high levels of probe expression (Fig S1E). Analysis was therefore restricted to cells expressing moderate levels of the biosensor (≤ 400 a.u./cell).

We first analyzed RhoA activation in MTLn3 cells under steady-state conditions, moving randomly in 5% serum, using live time-lapse FRET ratio imaging. RhoA activation was found to localize to the protruding edges of spontaneously moving cells (Figure 1D, upper panel and Supplemental movie S1). These images unambiguously define newly formed protrusion, and confirm the localization of RhoA to these sites. In order to obtain higher temporal resolution of RhoA activation, we collected time-lapse images of cells after acute EGF stimulation. RhoA activation was biphasic, with peaks of activity at 1 and 3 min at the tip of actively protruding lamellipodia (Figure 1D, lower panel, Fig. 1E, and Supplemental Movie S2).

### Inhibition of the Rho/ROCK pathway leads to decreased motility but enhanced protrusion

The finding of RhoA activation at the front of protruding MTLn3 cells suggested a role in motility that is not confined to the regulation of tail retraction. We therefore tested the effects

of inhibiting Rho and its downstream effector p160ROCK [37] on cell motility. Inhibition of either Rho by microinjection of cells with C3T led to a substantial decrease in cell motility in serum (Table 1). Similarly results were obtained in cells treated with the ROCK inhibitor Y27632. (Although Y27632 inhibits Rock-I, Rock-II, and PRK, its affects on wound healing and protrusion are mimicked by knockdown of ROCK-I but not ROCK-II or PRK-2 [38]). Whereas control cells undergoing cell motility in serum extended lamellipodia preferentially in the direction of movement, the C3T-injected cells and the Y27632-treated cells protruded in all directions and adopted a round flat morphology, which led to the cells being nearly stationary (Supplemental movies S3 and S4).

We next measured the effect of Rho/ROCK inhibition on acute EGF-stimulated protrusion. MTLn3 cells stimulated with EGF show an increase in cell area due to actin-mediated protrusion. In contrast, MTLn3 cells microinjected with the Rho inhibitor C3T showed a basal cell area that was comparable to the final area of control EGF-stimulated cells; C3T-injected cells extended only slightly more in response to EGF (Figure 2A and 2B). Actin staining of the EGF-stimulated C3T-microinjected cells showed a loss of actin stress fibers, but still show an accumulation of F-actin at the cell edge (Fig. 2A). These data suggest that inhibition of Rho is sufficient to induce protrusion in MTLn3 cells. A related phenotype was seen in cells treated with the ROCK inhibitor Y27632. While treatment of cells with Y27632 had no effect on the cell area of unstimulated cells, Y27632-treated cells showed hyperextension in response to EGF stimulation (Figures 2C, 2D). This phenotype was not seen in a previous study using lower doses of Y27632 that were sufficient to inhibit cofilin phosphorylation but only partially inhibited ROCK, as assessed by residual EGF-stimulated LIM kinase phosphorylation [39]. Thus, inhibition of Rho or ROCK led to basal or EGF-stimulated hyperextension, respectively.

The broad area of RhoA activation that we detected after 3 min of EGF stimulation is similar to the localization of phosphorylated myosin light chain, which is regulated by myosin light chain kinase and ROCK [40]. To test whether the effect of Rho/ROCK inhibition on protrusion was due to a disruption of the contractile apparatus, we treated the cells with the myosin light chain kinase inhibitor ML-7. However, no changes in basal or EGF-stimulated protrusion were observed (Fig. S2.A); controls showed that the drug was active, as it blocked myosin light chain phosphorylation in EGF-stimulated MDA-MB-231 cells (Fig. S2.B) [41]. Similarly, we saw no effects on overall EGF receptor signaling, as measured by activation of Akt and Erk (Fig. S2.C).

## Inhibition of ROCK hyperactivates Rac

The hyperprotrusion caused by inhibition of ROCK (Fig. 3A, panel 3) resembles the phenotype of MTLn3 cells expressing constitutively active Rac1, which leads to constitutive protrusion (Fig. 3A, panel 4) but decreased motility (Table 2). We therefore tested whether Rho inhibition might enhance protrusion through affects on Rac1 (Rac 2 and Rac 3 expression is barely detectable in MTLn3 cells [26]). MTLn3 cells microinjected with C3T (Fig. 3B, right panels) or treated with the ROCK inhibitor (Fig. 3C, right panels) showed a pronounced increase in Rac localization to the cell edge after 3 minutes of EGF stimulation. Rac localized to a broad area that spans the newly formed protrusion, reminiscent of the localization of activated RhoA in cells stimulated with EGF for 3 minutes (Figure 1B). The enhanced Rac localization at the cell edge reflected an increase in Rac activation, as measured by a Rac pull-down assay (Fig. 3D). In contrast, neither Cdc42 localization (data not shown) nor activation (Fig. S3) were affected by ROCK inhibition, similar to results in fibroblasts [42].

Rac mediates the formation of focal complexes, which then undergo Rho-mediated maturation into focal adhesions [13]. Given the hyperactivation of Rac in Y27632-treated cells, we examined the effects of ROCK inhibition of the EGF-stimulated formation of adhesive structures. In control cells stimulated with EGF for 3 min and stained for paxillin, a mixture

of focal complexes at the cell periphery and focal adhesions in the lamellar region of the cell can be seen (Fig. 4A, top panels). However, treatment of cells with Y27632 lead to a marked increase in focal complexes and a near total loss of focal adhesions (Figure 4A, bottom panels). The increase in focal complexes was presumably due to Rac hyperactivation, since knockdown of Rac1 abolished focal complex formation and focal adhesions in both control and Y27632-treated cells (Fig. 4B).

## Inhibition of ROCK leads to a switch from Cdc42-dependent to Rac1-dependent protrusion

We have previously shown that in control MTLn3 cells, EGF-stimulated protrusion is unaffected by knockdown of Rac1 [43], but is inhibited by knockdown of Cdc42 [24]. Given the dramatic increase in Rac1 activation caused by inhibition of ROCK, we tested whether the functional roles of Rac and Cdcd42 were altered in Y27632-treated cells. As previously noted, knockdown of Rac1 (Fig. 5A) has minimal effect on protrusion in MTLn3 cells (Figure 5C, white versus light grey bars). However, protrusion in the presence of Y27632 was markedly suppressed by Rac1 knockdown (Figure 5B, and 5C, dark grey versus black bars). These data were replicated using a distinct pool of four Rac1 siRNA oligos (Fig. S4A). Similarly, as previously reported, knockdown of Cdc42 in control MTLn3 cells markedly suppresses EGF-stimulated protrusion (Fig. 6B, white versus light grey bars). However, Cdc42 knockdown cells treated with Y27632 still showed enhanced protrusion relative to control cells (Fig. 6A and 6B, black versus white bars). Some inhibition of protrusion by Cdc42 knockdown is seen at 1 min, but this may be secondary to an inhibition of Rac membrane translocation that is seen at 1 but not 3 min (Fig. S4B). As previously shown [24], Cdc42 knockdown in control MTLn3 cells leads to a complete loss of the lamellipodial region, as the tropomyosin-rich lamellar region [30,36] extends to the cell edge (Fig. 6C, left panels). In contrast, the tropomyosin free, Arp2/3-rich lamellipodial compartment is clearly visible in both control and Cdc42 knockdown cells treated with Y27632 (Fig. 6C, right hand panels). Thus, Cdc42 is required for protrusion and maintenance of normal lamellipodial architecture is control cells, and this dependence is eliminated by inhibition of ROCK.

## MTC cells show decreased Rho activation and Rac-dependent protrusion

To test the hypothesis that Cdc42-dependent and Rac-independent protrusion in MTLn3 cells is related to high Rho activity, we examined the related non-metastatic carcinoma line, MTC [44,45]. MTC cells have previously been shown to move faster and to be more intrinsically polarized than MTLn3 cells [46]. Since native MTC cells do not respond to EGF, we used cells expressing the EGF receptor [25].

As shown in Fig. 7A and Supplemental Movie S5, MTC cells moving in serum show decreased levels of RhoA activation at the edge of protrusions as compared to MTLn3 cells. Similarly, both GTP-bound and total Rho is decreased in MTC cells relative to MTLn3 cells in a pull-down assay (Fig. 7B). We next tested whether inhibition of ROCK would lead to an increase in Rac activation, as it did in MTLn3 cells. Interestingly, we found that Rac activity in MTC cells was elevated as compared to MTLn3 cells, and was unaffected by inhibition of ROCK; EGF-stimulated Rac activity in MTC cells was similar to EGF-Rac activity in Y27632-treated MTLn3 cells. Thus, in MTC cells we find decreased RhoA activity, increased Rac activity, and a failure of ROCK inhibition to lead to additional activation Rac.

Given that finding of low RhoA activity and high Rac activity in MTC cells relative to MTLn3 cells, we tested whether Rac would be required for protrusion in MTC cells. We knocked down Rac1 expression in MTC cells (Fig. 7D) and recorded time-lapse images of control or Rac1 siRNA-treated cells (Supplemental Movie S6; representative images in Fig. 7E). MTC cells treated with Rac1 siRNA were less well spread than cells treated with control siRNA, and in contrast to MTLn3 cells [26], showed a marked decrease in EGF-stimulated protrusion (Fig.

7F). Thus, in MTLn3 cells, where we find increased RhoA activity and decreased Rac activity, protrusion is Cdc42-dependent and Rac-independent [24,26]; Rac activity and Rac-dependent protrusion is restored upon inhibition of ROCK (Fig. 6). In contrast, MTC cells exhibit decreased RhoA activity, increased Rac activity, and Rac-dependent protrusion (Fig. 7). These data suggest that RhoA-mediated inhibition of Rac activity determines the relative contribution of Rac and Cdc42 to EGF-stimulated protrusion.

## Discussion

In this report, we have examined the role of RhoA in MTLn3 rat adenocarcinoma cells. We find that RhoA follows a biphasic activation profile in EGF-stimulated cells, with an early activation peak at 1 minute and a late phase of activation after 3 minutes. Thus, RhoA activation is coincident with barbed end formation in MTLn3 cells in response to EGF stimulation [2]. The finding of activated RhoA in EGF-stimulated protrusions is consistent with recent reports implicating RhoA activity at the leading edge of moving cells [17,19,47,48].

In MTLn3 carcinoma cells, EGF-stimulated lamellipodial protrusion requires activation of Ras and Cdc42, but not Rac [24,43]. This is in contrast to fibroblasts, where Rac but not Cdc42 is the major positive regulator of protrusion [5]. Interestingly, we find that Rho and ROCK are not required for protrusion, and their inhibition in fact leads to an increase in protrusion. Instead, Rho and ROCK regulate the coupling of Rac versus Cdc42 to the protrusive machinery. Thus, in control MTLn3 cells, knockdown of Cdc42 but not Rac inhibits protrusion, whereas in Y27632-treated MTLn3 cells, knockdown of Rac1 but not Cdc42 blocks protrusion. The Rho/ROCK-mediated maintenance of Cdc42-dependent protrusion is apparently due to its inhibition of Rac-1, since inhibition of ROCK markedly increases Rac1 activity but has little effect on Cdc42. Rho-Rac antagonism has been observed in other cell models [49] and may reflect activation of a Rac GAP such as FilGAP, which is activated by RhoA and ROCK [50]. However, a role for Rho in switching a cell between Cdc42- versus Rac-mediated protrusion has not been previously described.

The phenotypes of Rho and ROCK inhibition are not identical: Rho inhibition led to constitutive circumferential protrusion, whereas ROCK inhibition led to an exaggeration of EGF-stimulated protrusion. This difference presumably reflects the contribution of additional downstream Rho effectors that are not affected by inhibition of ROCK, which might inhibit protrusion under basal conditions but enhance protrusion during EGF stimulation.

Despite increased protrusion, inhibition of Rho or ROCK leads to decreased motility in 2D culture, consistent with data from colon cancer cells [51] but different from studies in MDA-MB-231 adenocarcinoma cells [52]. The loss of motility in C3T- or Y27632-treated MTLn3 cells could be in part due to excessive Rac activation, as expression of a constitutively active Rac mutant in MTLn3 (Table 2) and other cells lines [53] leads to a symmetrical, circumferential protrusion and decreased motility. The effects of Rho/ROCK inhibition on motility could also be due in part to changes in the regulation of adhesive structures, as maturation of focal adhesions is blocked by inhibition of ROCK, consistent with previous studies [13].

Our data suggest a model in which variation in the amplitude of RhoA signaling can regulate motility through its inhibitory effects of Rac1. Thus, cells with lower levels of RhoA activity may show an increased Rac activity and a greater dependence on Rac for control of protrusion. Consistent with this model, we find that MTC carcinoma cells, a non-metastatic cell line closely related to MTLn3 cells, shows lower RhoA activity, higher Rac activity, and Rac-dependent protrusion. Thus, variation in the amplitude of Rho/ROCK activation in response to chemotactic stimuli may orchestrate the relative roles of Rac1 and Cdc42 during protrusion.

## Supplementary Material

Refer to Web version on PubMed Central for supplementary material.

## Acknowledgements

The authors would like to thank the Analytical Imaging Facility at Albert Einstein College of Medicine, particularly Mr. Michael Cammer for valuable discussions and technical help with image analysis. We would also like to thank Dr. Stefan Huettelmaier for providing the GFP-vinculin and Dr. Anne Bresnick, Dr. Jeff Segall, and Dr. Louis Hodgson for valuable discussions. This work was supported by National Institutes of Health grant CA 100324 (J.C. and J.M.B.) and a grant from the Janey Fund (J.M.B.).

## References

1. Devreotes P, Janetopoulos C. Eukaryotic chemotaxis: distinctions between directional sensing and polarization. J Biol Chem 2003;278:20445–20448. [PubMed: 12672811]
2. Chan AY, Raft S, Bailly M, Wyckoff JB, Segall JE, Condeelis JS. EGF stimulates an increase in actin nucleation and filament number at the leading edge of the lamellipod in mammary adenocarcinoma cells. J Cell Sci 1998;111(Pt 2):199–211. [PubMed: 9405304]
3. Condeelis JS, Wyckoff JB, Bailly M, Pestell R, Lawrence D, Backer J, Segall JE. Lamellipodia in invasion. Semin Cancer Biol 2001;11:119–128. [PubMed: 11322831]
4. Ridley AJ. Rho family proteins: coordinating cell responses. Trends Cell Biol 2001;11:471–477. [PubMed: 11719051]
5. Nobes CD, Hall A. Rho, rac, and cdc42 GTPases regulate the assembly of multimolecular focal complexes associated with actin stress fibers, lamellipodia, and filopodia. Cell 1995;81:53–62. [PubMed: 7536630]
6. Eden S, Rohatgi R, Podtelejnikov AV, Mann M, Kirschner MW. Mechanism of regulation of WAVE1-induced actin nucleation by Rac1 and Nck. Nature 2002;418:790–793. [PubMed: 12181570]
7. Rohatgi R, Ma L, Miki H, Lopez M, Kirchhausen T, Takenawa T, Kirschner MW. The interaction between N-WASP and the Arp2/3 complex links Cdc42-dependent signals to actin assembly. Cell 1999;97:221–231. [PubMed: 10219243]
8. Takaishi K, Kikuchi A, Kuroda S, Kotani K, Sasaki T, Takai Y. Involvement of rho p21 and its inhibitory GDP/GTP exchange protein (rho GDI) in cell motility. Mol Cell Biol 1993;13:72–79. [PubMed: 8417362]
9. Hakuma N, Kinoshita I, Shimizu Y, Yamazaki K, Yoshida K, Nishimura M, Dosaka-Akita H. E1AF/PEA3 activates the Rho/Rho-associated kinase pathway to increase the malignancy potential of non-small-cell lung cancer cells. Cancer Res 2005;65:10776–10782. [PubMed: 16322223]
10. Worthylake RA, Lemoine S, Watson JM, Burridge K. RhoA is required for monocyte tail retraction during transendothelial migration. J Cell Biol 2001;154:147–160. [PubMed: 11448997]
11. Raftopoulou M, Hall A. Cell migration: Rho GTPases lead the way. Dev Biol 2004;265:23–32. [PubMed: 14697350]
12. Chrzanowska-Wodnicka M, Burridge K. Rho-stimulated contractility drives the formation of stress fibers and focal adhesions. J Cell Biol 1996;133:1403–1415. [PubMed: 8682874]
13. Rottner K, Hall A, Small JV. Interplay between Rac and Rho in the control of substrate contact dynamics. Curr Biol 1999;9:640–648. [PubMed: 10375527]
14. Pertz O, Hodgson L, Klemke RL, Hahn KM. Spatiotemporal dynamics of RhoA activity in migrating cells. Nature 2006;440:1069–1072. [PubMed: 16547516]
15. Pertz O, Hahn KM. Designing biosensors for Rho family proteins--deciphering the dynamics of Rho family GTPase activation in living cells. J Cell Sci 2004;117:1313–1318. [PubMed: 15020671]
16. Benink HA, Bement WM. Concentric zones of active RhoA and Cdc42 around single cell wounds. J Cell Biol 2005;168:429–439. [PubMed: 15684032]
17. O'Connor KL, Nguyen BK, Mercurio AM. RhoA function in lamellae formation and migration is regulated by the alpha6beta4 integrin and cAMP metabolism. J Cell Biol 2000;148:253–258. [PubMed: 10648558]

18. Cho SY, Klemke RL. Purification of pseudopodia from polarized cells reveals redistribution and activation of Rac through assembly of a CAS/Crk scaffold. J Cell Biol 2002;156:725–736. [PubMed: 11839772]

19. Kurokawa K, Matsuda M. Localized RhoA activation as a requirement for the induction of membrane ruffling. Mol Biol Cell 2005;16:4294–4303. [PubMed: 15987744]

20. Amano M, Chihara K, Kimura K, Fukata Y, Nakamura N, Matsuura Y, Kaibuchi K. Formation of actin stress fibers and focal adhesions enhanced by Rho-kinase. Science 1997;275:1308–1311. [PubMed: 9036856]

21. Wyckoff JB, Pinner SE, Gschmeissner S, Condeelis JS, Sahai E. ROCK- and myosin-dependent matrix deformation enables protease-independent tumor-cell invasion in vivo. Curr Biol 2006;16:1515–1523. [PubMed: 16890527]

22. Maekawa M, Ishizaki T, Boku S, Watanabe N, Fujita A, Iwamatsu A, Obinata T, Ohashi K, Mizuno K, Narumiya S. Signaling from Rho to the actin cytoskeleton through protein kinases ROCK and LIM-kinase. Science 1999;285:895–898. [PubMed: 10436159]

23. Higashida C, Miyoshi T, Fujita A, Oceguera-Yanez F, Monypenny J, Andou Y, Narumiya S, Watanabe N. Actin polymerization-driven molecular movement of mDia1 in living cells. Science 2004;303:2007–2010. [PubMed: 15044801]

24. El-Sibai M, Nalbant P, Pang H, Flinn RJ, Sarimento C, Macaluso F, Cammer M, Condeelis JS, Hahn KM, Backer JM. Cdc42 is Required for EGF-Stimulated Protrusion and Motility in MTLn3 Carcinoma Cells. J Cell Sci 2007;120:3465–3474. [PubMed: 17855387]

25. Wyckoff JB, Insel L, Khazaie K, Lichtner RB, Condeelis JS, Segall JE. Suppression of ruffling by the EGF receptor in chemotactic cells. Exp Cell Res 1998;242:100–109. [PubMed: 9665807]

26. Yip SC, El-Sibai M, Coniglio SJ, Mouneimne G, Eddy RJ, Drees BE, Neilsen PO, Goswami S, Symons M, Condeelis JS, Backer JM. The distinct roles of Ras and Rac in PI 3-kinase-dependent protrusion during EGF-stimulated cell migration. J Cell Sci 2007;120:3138–3146. [PubMed: 17698922]

27. Yamaguchi H, Lorenz M, Kempiak S, Sarmiento C, Coniglio S, Symons M, Segall J, Eddy R, Miki H, Takenawa T, Condeelis J. Molecular mechanisms of invadopodium formation: the role of the N-WASP-Arp2/3 complex pathway and cofilin. J Cell Biol 2005;168:441–452. [PubMed: 15684033]

28. Chan AY, Coniglio SJ, Chuang YY, Michaelson D, Knaus UG, Philips MR, Symons M. Roles of the Rac1 and Rac3 GTPases in human tumor cell invasion. Oncogene 2005;24:7821–7829. [PubMed: 16027728]

29. Eddy RJ, Pierini LM, Matsumura F, Maxfield FR. Ca2+-dependent myosin II activation is required for uropod retraction during neutrophil migration. J Cell Sci 2000;113(Pt 7):1287–1298. [PubMed: 10704379]

30. DesMarais V, Ichetovkin I, Condeelis J, Hitchcock-DeGregori SE. Spatial regulation of actin dynamics: a tropomyosin-free, actin-rich compartment at the leading edge. J Cell Sci 2002;115:4649–4660. [PubMed: 12415009]

31. Wessels D, Voss E, Von Bergen N, Burns R, Stites J, Soll DR. A computer-assisted system for reconstructing and interpreting the dynamic three-dimensional relationships of the outer surface, nucleus and pseudopods of crawling cells. Cell Motil Cytoskeleton 1998;41:225–246. [PubMed: 9829777]

32. Miyawaki A, Tsien RY. Monitoring protein conformations and interactions by fluorescence resonance energy transfer between mutants of green fluorescent protein. Methods Enzymol 2000;327:472–500. [PubMed: 11045004]

33. Ren XD, Kiosses WB, Schwartz MA. Regulation of the small GTP-binding protein Rho by cell adhesion and the cytoskeleton. EMBO J 1999;18:578–585. [PubMed: 9927417]

34. Bailly M, Condeelis JS, Segall JE. Chemoattractant-induced lamellipod extension. Microsc Res Tech 1998;43:433–443. [PubMed: 9858340]

35. Adamson P, Paterson HF, Hall A. Intracellular localization of the P21rho proteins. J Cell Biol 1992;119:617–627. [PubMed: 1383236]

36. Gupton SL, Anderson KL, Kole TP, Fischer RS, Ponti A, Hitchcock-DeGregori SE, Danuser G, Fowler VM, Wirtz D, Hanein D, Waterman-Storer CM. Cell migration without a lamellipodium:

translation of actin dynamics into cell movement mediated by tropomyosin. J Cell Biol 2005;168:619–631. [PubMed: 15716379]

37. Worthylake RA, Burridge K. RhoA and ROCK promote migration by limiting membrane protrusions. J Biol Chem 2003;278:13578–13584. [PubMed: 12574166]
38. Darenfed H, Dayanandan B, Zhang T, Hsieh SH, Fournier AE, Mandato CA. Molecular characterization of the effects of Y-27632. Cell Motil Cytoskeleton 2007;64:97–109. [PubMed: 17009325]
39. Song X, Chen X, Yamaguchi H, Mouneimne G, Condeelis JS, Eddy RJ. Initiation of cofilin activity in response to EGF is uncoupled from cofilin phosphorylation and dephosphorylation in carcinoma cells. J Cell Sci 2006;119:2871–2881. [PubMed: 16803871]
40. Matsumura F, Ono S, Yamakita Y, Totsukawa G, Yamashiro S. Specific localization of serine 19 phosphorylated myosin II during cell locomotion and mitosis of cultured cells. J Cell Biol 1998;140:119–129. [PubMed: 9425160]
41. Dulyaninova NG, House RP, Betapudi V, Bresnick AR. Myosin-IIA Heavy-Chain Phosphorylation Regulates the Motility of MDA-MB-231 Carcinoma Cells. Mol Biol Cell 2007;18:3144–3155. [PubMed: 17567956]
42. Nalbant P, Hodgson L, Kraynov V, Toutchkine A, Hahn KM. Activation of endogenous Cdc42 visualized in living cells. Science 2004;305:1615–1619. [PubMed: 15361624]
43. Yip SC, Backer JM, et al. The Distinct Roles of Ras and Rac in PI 3-Kinase Dependent Protrusion During EGF-Stimulated Cell Migration. Journal of Cell Science. 2007(in press)
44. Neri A, Welch D, Kawaguchi T, Nicolson GL. Development and biologic properties of malignant cell sublines and clones of a spontaneously metastasizing rat mammary adenocarcinoma. J Natl Cancer Inst 1982;68:507–517. [PubMed: 6950180]
45. Wyckoff JB, Jones JG, Condeelis JS, Segall JE. A critical step in metastasis: in vivo analysis of intravasation at the primary tumor. Cancer Res 2000;60:2504–2511. [PubMed: 10811132]
46. Shestakova EA, Wyckoff J, Jones J, Singer RH, Condeelis J. Correlation of beta-actin messenger RNA localization with metastatic potential in rat adenocarcinoma cell lines. Cancer Res 1999;59:1202–1205. [PubMed: 10096548]
47. Kurokawa K, Nakamura T, Aoki K, Matsuda M. Mechanism and role of localized activation of Rho-family GTPases in growth factor-stimulated fibroblasts and neuronal cells. Biochem Soc Trans 2005;33:631–634. [PubMed: 16042560]
48. Nishiyama T, Sasaki T, Takaishi K, Kato M, Yaku H, Araki K, Matsuura Y, Takai Y. rac p21 is involved in insulin-induced membrane ruffling and rho p21 is involved in hepatocyte growth factor- and 12-O-tetradecanoylphorbol-13-acetate (TPA)-induced membrane ruffling in KB cells. Mol Cell Biol 1994;14:2447–2456. [PubMed: 8139548]
49. Kozma R, Sarner S, Ahmed S, Lim L. Rho family GTPases and neuronal growth cone remodelling: Relationship between increased complexity induced by Cdc42Hs, Rac1, and acetylcholine and collapse induced by RhoA and lysophosphatidic acid. Mol Cell Biol 1997;17:1201–1211. [PubMed: 9032247]
50. Ohta Y, Hartwig JH, Stossel TP. FilGAP, a Rho- and ROCK-regulated GAP for Rac binds filamin A to control actin remodelling. Nat Cell Biol 2006;8:803–814. [PubMed: 16862148]
51. Croft DR, Sahai E, Mavria G, Li S, Tsai J, Lee WM, Marshall CJ, Olson MF. Conditional ROCK activation in vivo induces tumor cell dissemination and angiogenesis. Cancer Res 2004;64:8994–9001. [PubMed: 15604264]
52. Torka R, Thuma F, Herzog V, Kirfel G. ROCK signaling mediates the adoption of different modes of migration and invasion in human mammary epithelial tumor cells. Exp Cell Res 2006;312:3857–3871. [PubMed: 17010335]
53. Pankov R, Endo Y, Even-Ram S, Araki M, Clark K, Cukierman E, Matsumoto K, Yamada KM. A Rac switch regulates random versus directionally persistent cell migration. J Cell Biol 2005;170:793–802. [PubMed: 16129786]

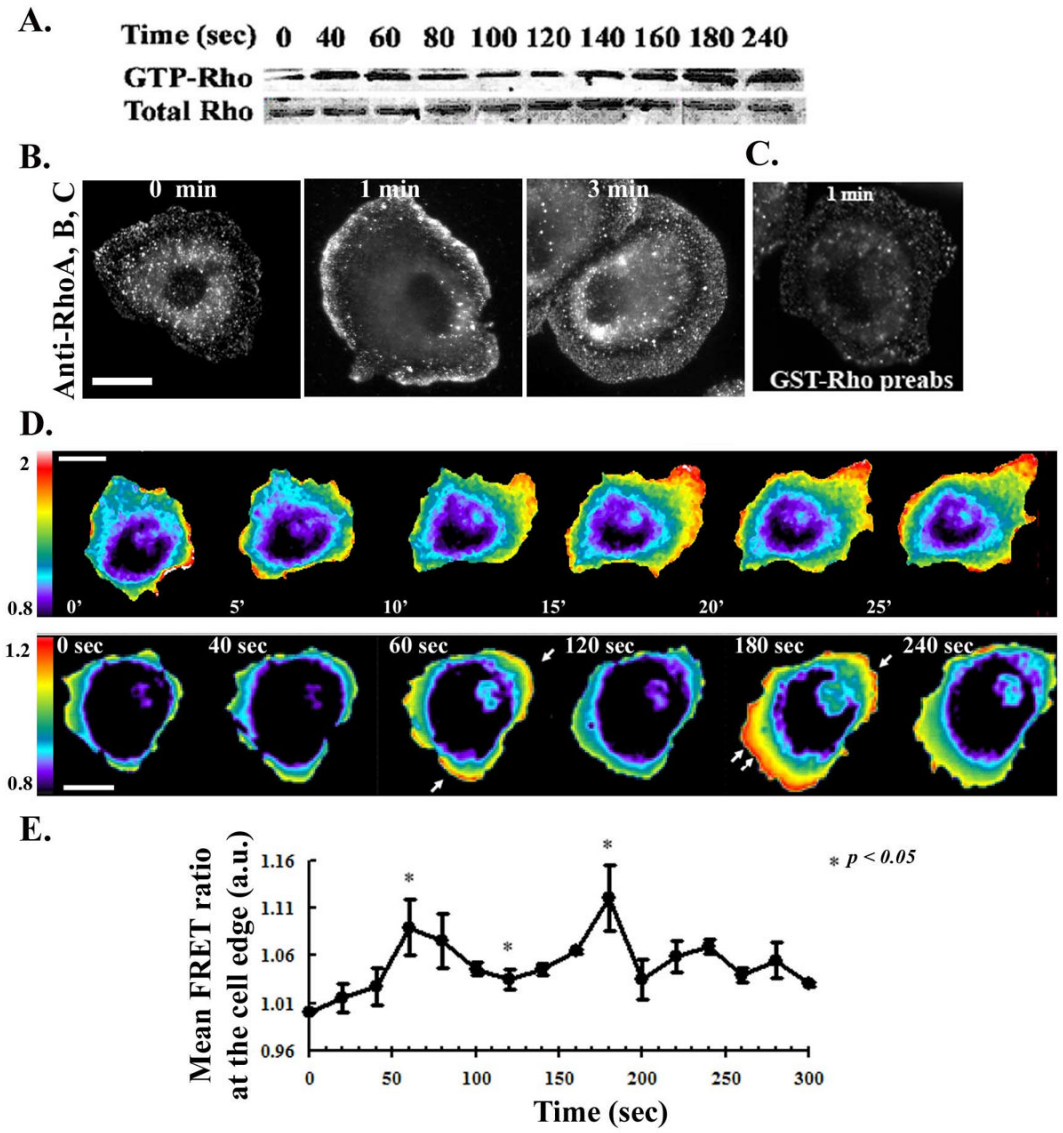


**Figure 1. Rho activation in EGF-stimulated carcinoma cells**

MTLn3 cells were starved for 3 hrs and stimulated with 5 nM EGF at 37°C for the indicated times. A) Representative Western blot of a GST-RBD pull-down showing Rho activation in MTLn3 cells. The lower gel shows the amount of total Rho in cell lysates. B) Representative fluorescent micrographs of MTLn3 cells stimulated with EGF and immunostained with anti-Rho antibody. C) Immunostaining of MTLn3 cells with anti-Rho antibody pre-absorbed with GST-Rho. D) Upper panels: Time-lapse FRET imaging of MTLn3 cells expressing the RhoA biosensor, moving randomly in 5% serum. Cells were imaged for CFP and FRET every minute for 30 minutes and the FRET/CFP ratios obtained (movie S1). Lower panels: FRET/CFP ratio of MTLn3 cells expressing the RhoA biosensor and stimulated with EGF. Images were collected every 20 seconds (movie S2 and S3). E) Measurements of the mean FRET ratio (ROI of 3 μm behind the leading edge) at various times after EGF stimulation, taken from the time lapse images. Data are the mean +/− SEM from 10 different cells. Scale bar is 10 μm.

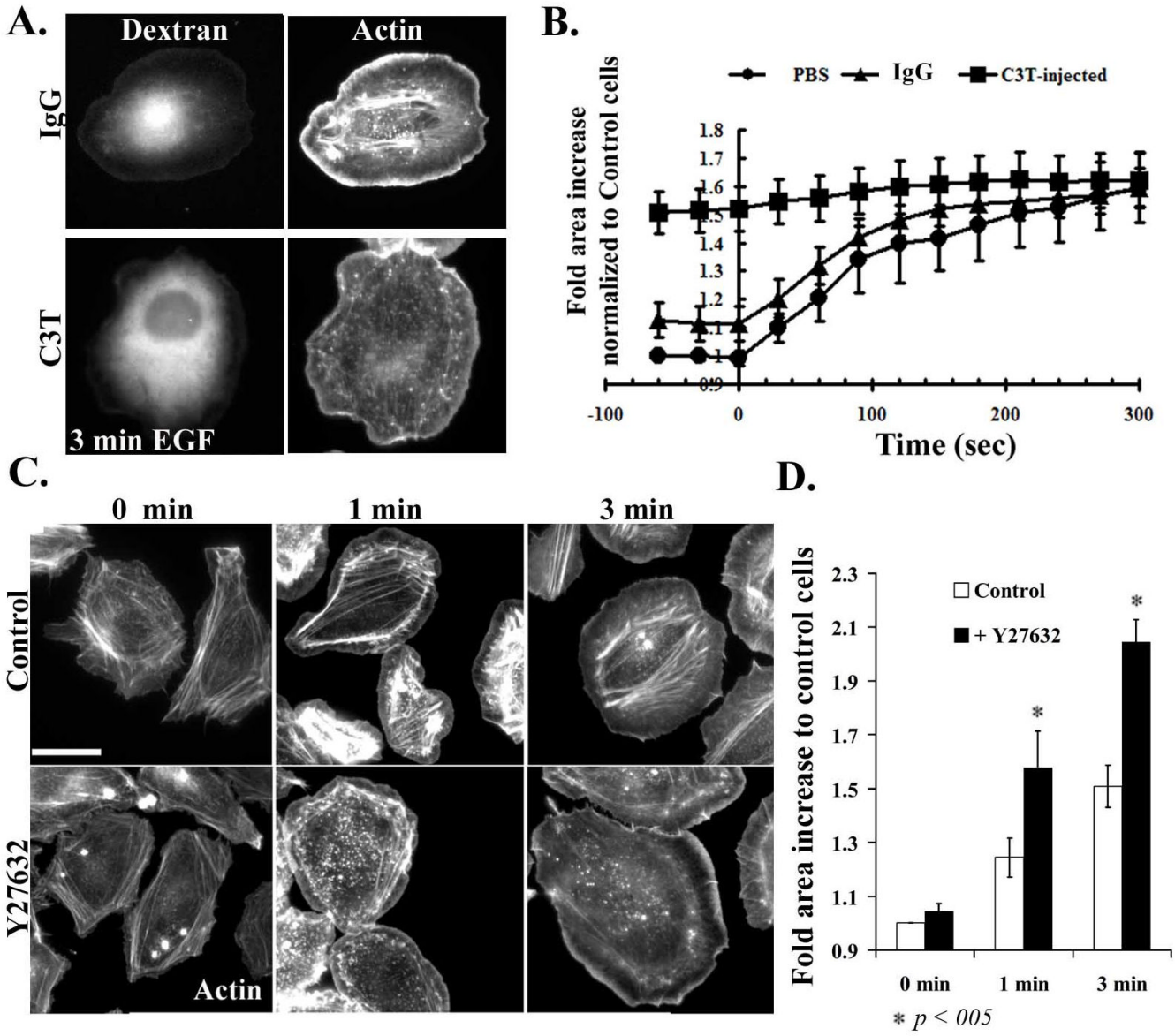


**Figure 2. Inhibition of Rho/ROCK leads to an increase in cell area**

A) Starved cells were microinjected with 488 Alexa-Dextran along with IgG control (upper panels) or with 150 μg/ml C3T along with Dextran (lower panels), allowed to recover for 1h, then fixed and stained with Rhodamine phalloidin. Left-hand panels show the 488Alexa fluorescence in microinjected cells and right-hand panels show f-actin staining. B) Control, IgG/dextran or C3T/dextran injected cells were stimulated with EGF and time lapses were performed, collecting images every 20 seconds. The surface area of control or injected cells was determined, and normalized to cells at time 0 before stimulation. Data are the mean +/− SEM from 20 cells. C) MTLn3 cells, plated on collagen, were starved for 3 hours and treated without or with 25 μM of Y27632 for 30 min. Cells are then stimulated with EGF for 0, 1 and 3 min, fixed and stained with Rhodamine Phalloidin. D) Quantitation of the surface areas of cells treated as in panel C, plotted as fold increase relative to control cells. The data are the mean from 3 +/− SEM from 3 different experiments (15 cells/experiment). Scale bar is 10 μm.

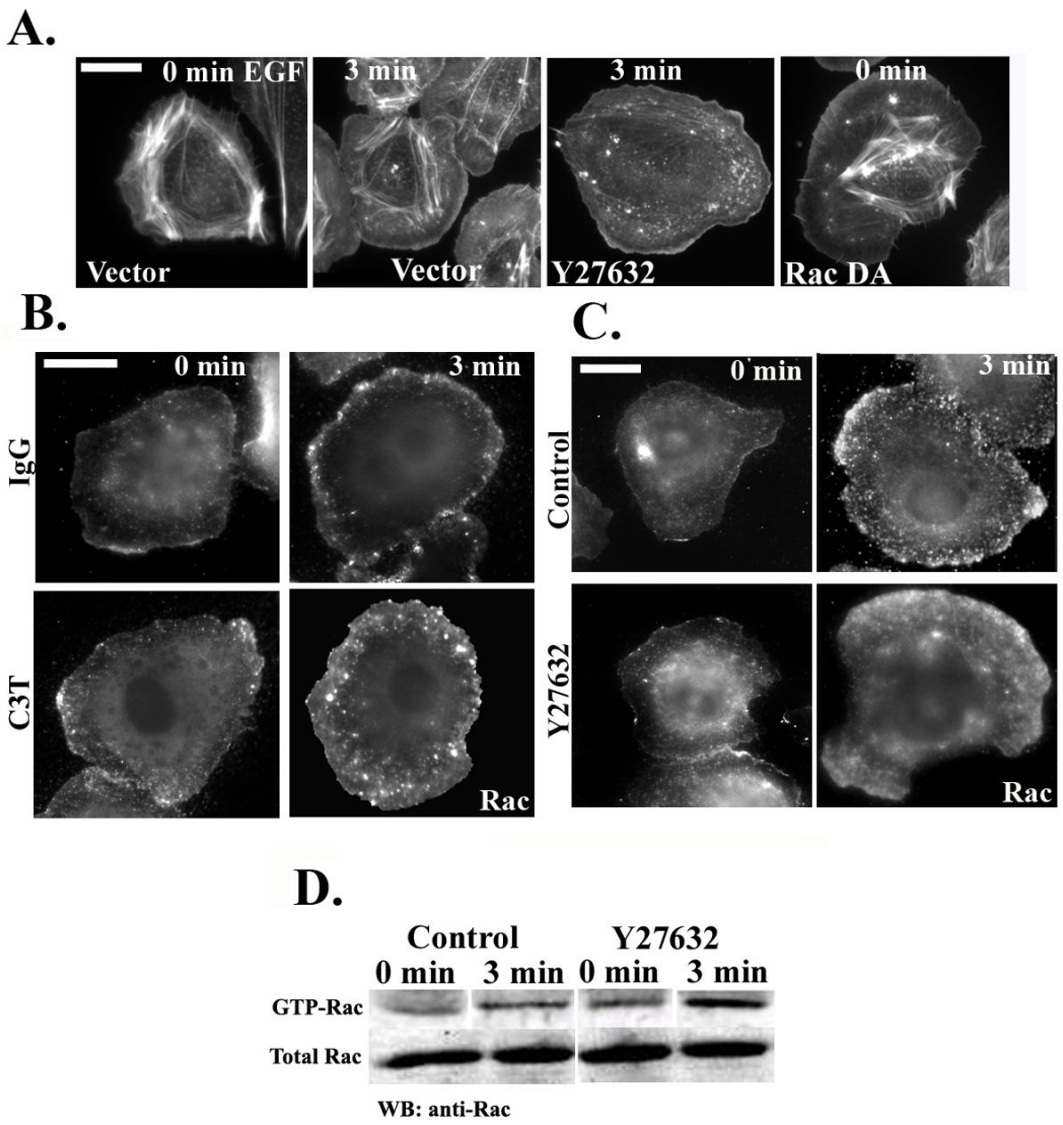


**Figure 3. Inhibition of RhoA/ROCK leads to Rac hyperactivation and increased membrane localization**

A) Rhodamine phalloidin staining of cells transfected with vector alone (first two panels), transfected with vector and treated with Y27632 (third panel) or transfected with RacQ61L (last panel to the right). Cells were starved for 3 hours, stimulated with EGF for 0 or 3 minutes, and stained with Rhodamine phalloidin. B) Representative micrographs of starved cells microinjected with 488Alexa-Dextran and IgG (upper panels) or 150 μg/ml C3T (lower panels). Cells were stimulated with EGF for 0 or 3 minutes and stained with anti-Rac antibodies. C) Representative micrographs of starved cells treated without or with carrier (upper panels) or Y27632 (25 μM; lower panels) for 30 min. Cells were stimulated with EGF for 0 or 3 minutes and stained with anti-Rac antibodies. D) GST-CRIB pull-down from control or Y27632-treated cells were blotted with anti-Rac antibody. The lanes for each blot (GTP and total Rac) were taken from the same gel.

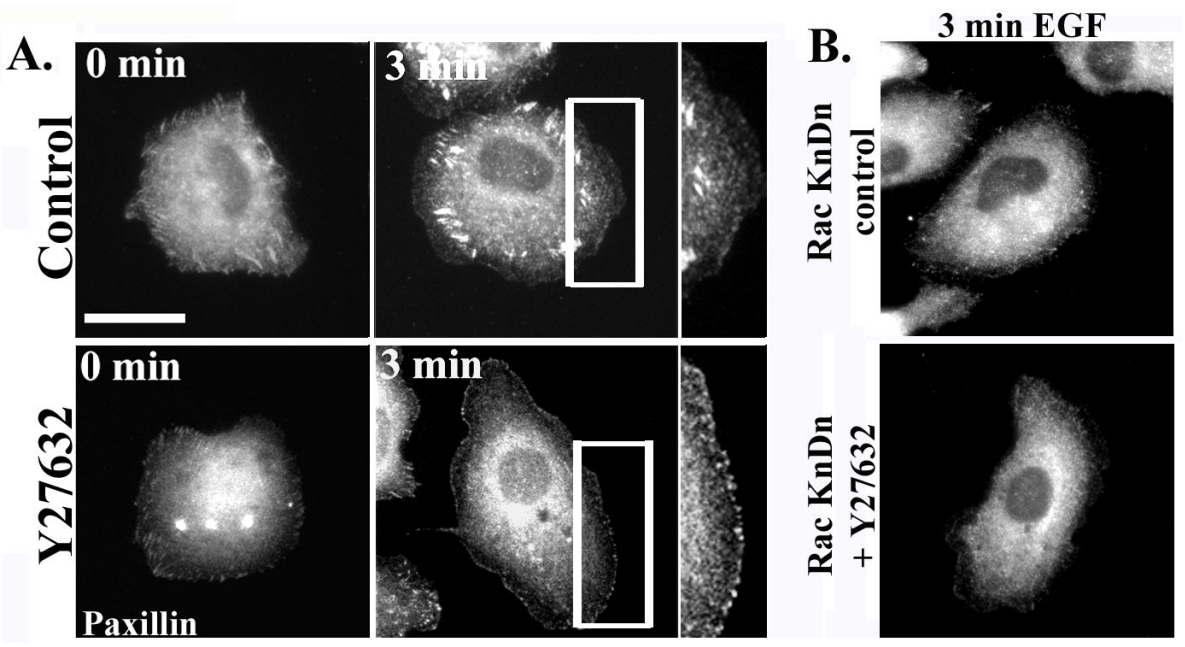


**Figure 4. ROCK inhibition blocks maturation of focal complexes to focal adhesions**

**A.** MTLn3 cells were starved for 3 hours, and then treated with carrier (upper panels) or with 25 μM of Y27632 (lower panels) for 30 minutes. Representative micrographs show cells stimulated with EGF for 0 or 3 minutes and stained for paxillin. B) Representative micrographs of MTLn3 cells transfected with Rac siRNA and treated with carrier (upper panel) or Y27632 (lower panel), stimulated with EGF for 3 minutes, and stained for paxillin.

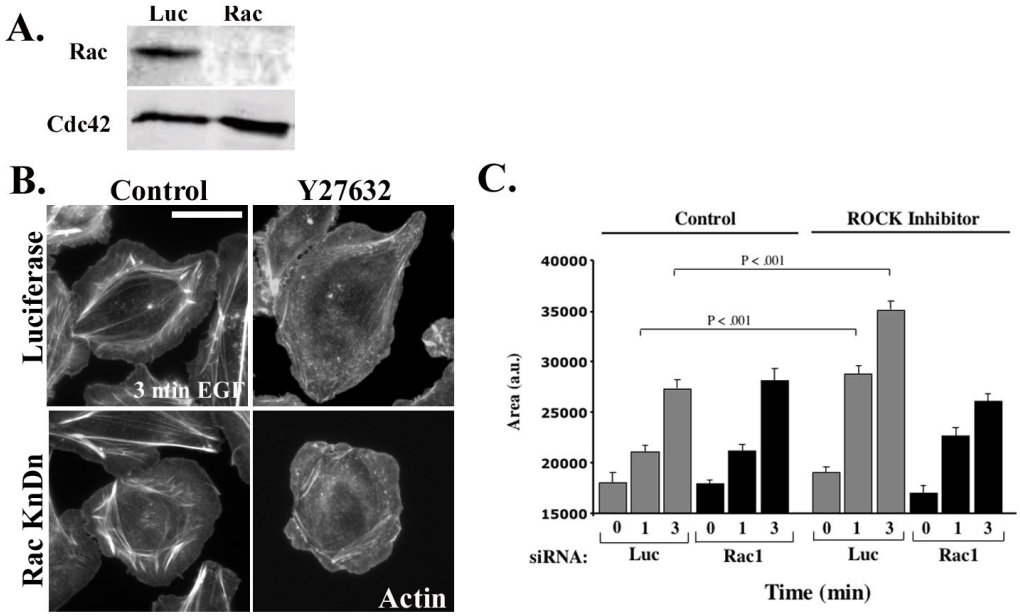


**Figure 5. EGF-stimulated protrusion in Y27632-treated cells is Rac dependent**

A) MTLn3 cells were transfected with control or Rac siRNA. Representative Western Blot showing the expression of Rac (upper panel) and Cdc42 (lower panel). B) Luciferase (upper panels) and Rac1 (lower panels) siRNA-treated cells were either incubated without or with 25 μM Y27632 for 30 min. The cells were then stimulated for 0, 1 and 3 minutes with EGF. The representative micrographs show cells stimulated for 3 minutes and stained with Rhodamine Phalloidin C) Quantitation of cells from (B) stimulated with EGF for 0,1 or 3 min. The data are normalized to the area of unstimulated control cells, and are the mean +/− SEM from at least 45 cells from three distinct experiments. Scale bar is 10 μm.

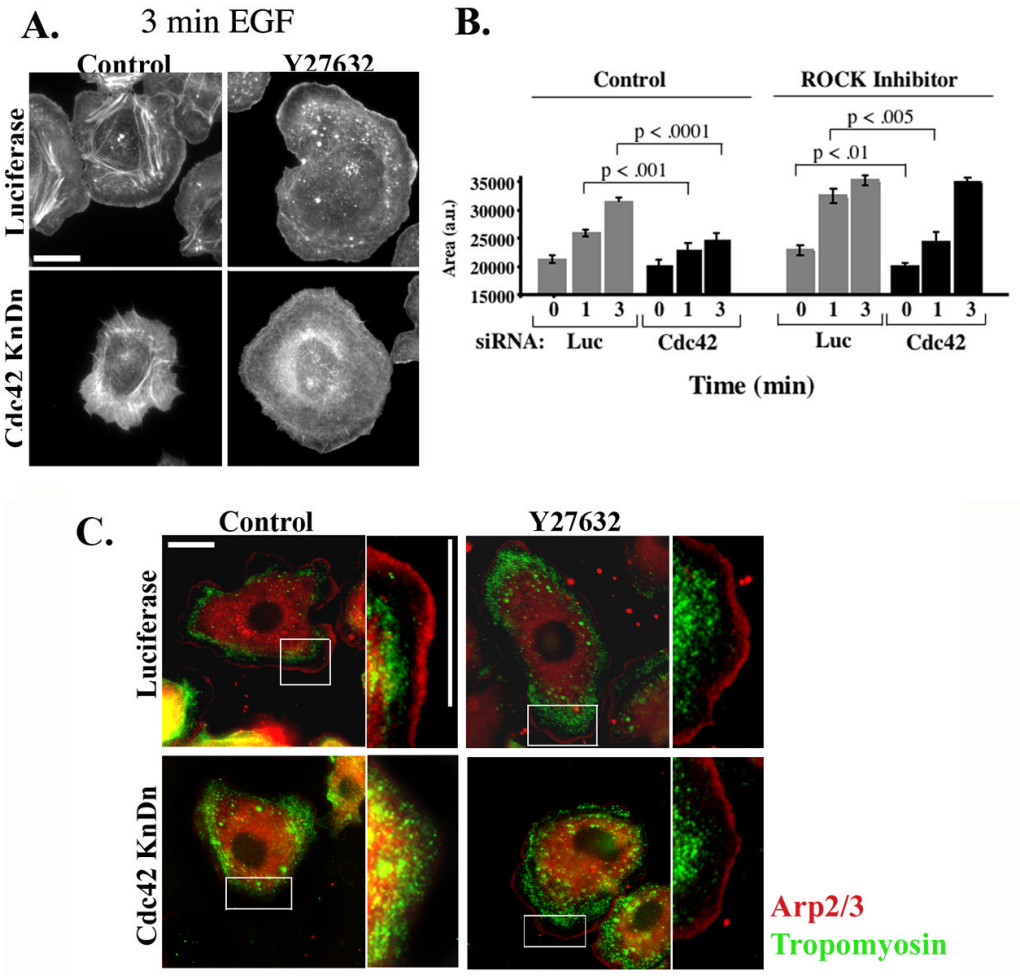


**Figure 6. EGF-stimulated protrusion in Y27632-treated cells is Cdc42-independent**

A) MTLn3 cells were transfected with Luciferase (upper panels) or with Cdc42 (lower panels) siRNA. Cells were starved for 3 hrs, treated with carrier (left panels) or 25 μM Y27632 (right panels) for 30 min, and stimulated for 0, 1 and 3 minutes with EGF. The representative micrographs show cells stimulated for 3 minutes and stained with Rhodamine Phalloidin. B) Quantitation of cells from (A) stimulated with EGF for 0,1 or 3 min. The data are normalized to the area of unstimulated control cells, and are the mean +/− SEM from at least 45 cells. Scale bar is 10 μm. C) MTLn3 cells were transfected with Luciferase (upper panels) or with Cdc42 (lower panels) siRNA. Cells were starved for 3 hrs, treated with carrier (left panels) or 25 μM Y27632 (right panels) for 30 min, and stimulated for 3 minutes with EGF. The cells were fixed and stained with anti-tropomyosin (green) or anti-p34 (red) antibodies.

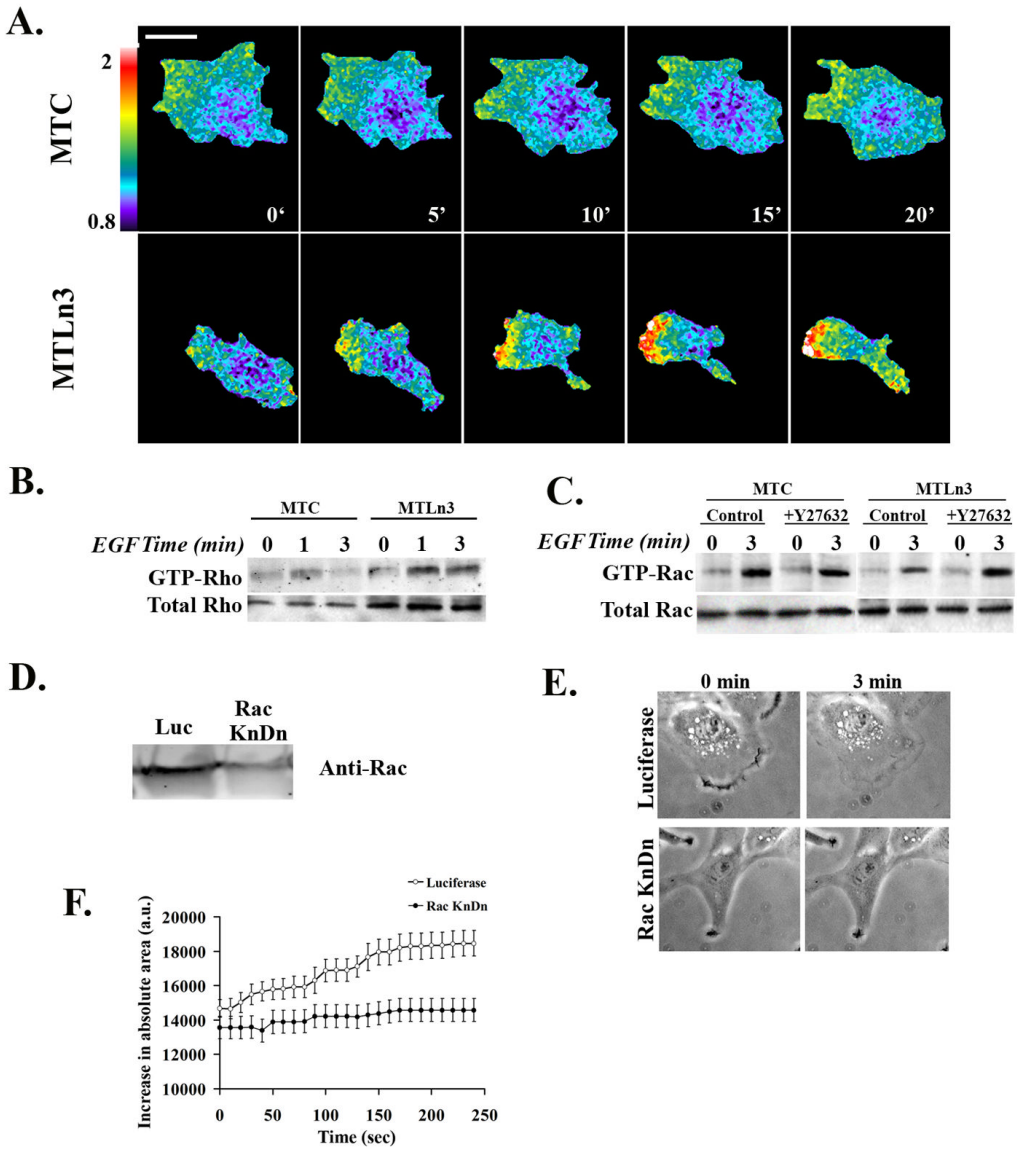


**Figure 7. MTC cells have decreased RhoA activity, increased Rac activity, and show Rac-dependent protrusion**

A) Time-lapse FRET imaging of MTC cells (upper panels) or MTLn3 cells (lower panels) expressing the RhoA biosensor, moving randomly in 5% serum. Cells were imaged for CFP and FRET every minute for 30 minutes and the FRET/CFP ratios obtained (movie S6). The data are representative of two independent experiments, and five time lapse series. B) Representative Western blot of a GST-RBD pull-down showing Rho activation in MTC and MTLn3 cells. The lower gels show the amount of total Rho in cell lysates. The data are representative of two independent experiments. C) GST-CRIB pull-downs from MTC or MTLn3 cells, treated with carrier or Y27632-treated, and blotted with anti-Rac antibody. Lower gels show total Rac in cell lysates. The data are representative of two independent experiments. D) Anti-Rac blot of lysates from control or Rac1 siRNA-treated MTC cells. E) Representative frames from time-lapse images of control or Rac1 siRNA-treated MTC cells, stimulated with EGF for 0 or 3 min (from Movie S7). F) Surface area of control or Rac1 siRNA-treated MTC cells, after stimulation with EGF. The data show the mean ± SEM from 10 cells per condition, from two separate experiments.

**Table 1**

**Inhibition of the Rho/ROCK pathway inhibits the motility of carcinoma cells**

MTLn3 cells were microinjected with IgG or with C3T (150 μg/ml) (movie S4) or treated without or with 25 μM Y27632 for 30 min (movie S5). The cells were imaged in medium containing 5 % FBS for 2 hours. The time interval between successive frames was 1 min. Motility parameters were calculated using DIAS software [28], and the data are the mean ± SEM from 15–40 cells per condition.

| | Total path (μm) | Net path (μm) |
|---|---|---|
| IgG control | 82.14 +/− 5.5 | 46.28+− 4.1 |
| C3T | 46.01 +/− 5.1 | 12.64 +/− 1.8 |
| | $p < 0.5$ | $p < 0.05$ |
| control | 57.18 +/− 2.6 | 24.76 +/− 1.7 |
| Y27632 | 36.45 +/− 1.2 | 7.25 +/− 0.7 |
| | $p < 0.00005$ | $p < 0.0005$ |

**Table 2**

**expression of constitutively active Rac inhibits the motility of carcinoma cells**

MTLn3 cells were transfected with GFP-CA-Rac. The cells were imaged in medium containing 5 % FBS for 2 hours. The time interval between successive frames was 1 min. Motility parameters were calculated using DIAS software [28], and the data are the mean ± SEM from 15 cells per condition.

| | Total path (μm) | Net path (μm) |
|---|---|---|
| control vector | 76.13 +/− 6.3 | 30.62 +/− 2.4 |
| CARac | 21.12 +/− 1.5 | 8.71 +/− 6.2 |
| | $p < 0.05$ | $p < 0.05$ |